FERROELECTRICS
2020, VOL. 560, 38–47
https://doi.org/10.1080/00150193.2020.1722881

Taylor & Francis
Taylor & Francis Group

Structure, ferroelectric and local piezoelectric properties of KNN-based perovskite ceramics

E. D. Politova[a,b], G. M. Kaleva[a,b], A. V. Mosunov[a], N. V. Sadovskaya[c], D. A. Kiselev[d], A. M. Kislyuk[d], T. S. Ilina[d], S. Yu. Stefanovich[a,e], and E. A. Fortalnova[f]

[a]L. Ya. Karpov Institute of Physical Chemistry, Moscow, Russia; [b]Semenov Institute of Chemical Physics, Russian Academy of Sciences, Moscow, Russia; [c]FSRC «Crystallography and Photonics» RAS, Moscow, Russia; [d]National University of Science and Technology "MISiS", Moscow, Russia; [e]Lomonosov Moscow State University, Moscow, Russia; [f]Russian University of Peoples' Friendship, Moscow, Russia

ABSTRACT

Structure, microstructure, dielectric, ferroelectric, and local piezoelectric properties of perovskite ceramics in the systems $(1\text{-}x)(K_{0.5}Na_{0.5})NbO_3 - x(Bi_{0.5}Na_{0.5})TiO_3$ ($x = 0 \div 0.1$) and $(1\text{-}x)(K_{0.5}Na_{0.5})NbO_3 - x(Bi_{0.5}Na_{0.5})ZrO_3$ ($x = 0.01 \div 0.05$) have been studied. Improvement of dielectric parameters and effective d_{33} piezoelectric coefficient was obtained in compositions with $x = 0.03$ and 0.05, correspondingly.

ARTICLE HISTORY
Received 28 August 2019
Accepted 25 November 2019

KEYWORDS
Perovskite structure; $(Ka_{0.5}Na_{0.5})NbO_3$; $(Bi_{0.5}Na_{0.5})TiO_3$; $(Bi_{0.5}Na_{0.5})ZrO_3$; dielectric; ferroelectric; local piezoelectric properties

1. Introduction

Lead-free ferroelectric materials based on potassium-sodium niobate (K,Na)NbO_3 (KNN) perovskites are being intensively studied as they are considered among the most promising materials for replacement of piezoelectric ones containing toxic lead oxide [1–26]. However, difficulties in preparation of stoichiometric compositions due to sodium and potassium high volatility in course of narrow sintering temperature interval prevented commercialization of KNN-based materials [10–18].

Influence of various cation substitutions on structure and functional properties was studied in the systems on the base of sodium-potassium niobate $(K_{0.5}Na_{0.5})NbO_3$ (KNN) [14–26]. Initial KNN samples are characterized by the orthorhombic (O) phase at room temperature transforming to the tetragonal (T) and then to a paraelectric one with increasing temperature [9–11]. It was proved that various A- and B-sublattices dopants could enhance piezoelectricity in KNN-based compositions by shifting temperature of the transition from orthorhombic phase to tetragonal one to room temperature [16–20].

However, usually, Morphotropic Phase Boundary (MPB) in KNN-based compositions depends on temperature and phase coexistence and high d_{33} values are not maintained at increasing temperature. In particular, good piezoelectric properties were revealed in compositions $(1\text{-}x)(K_{1\text{-}y}Na_y)NbO_3 - x(Bi_{1/2}Na_{1/2})ZrO_3$ at room temperature [20]. However, a dramatic decrease in properties with increasing temperature was observed.

CONTACT E. D. Politova politova@nifhi.ru.

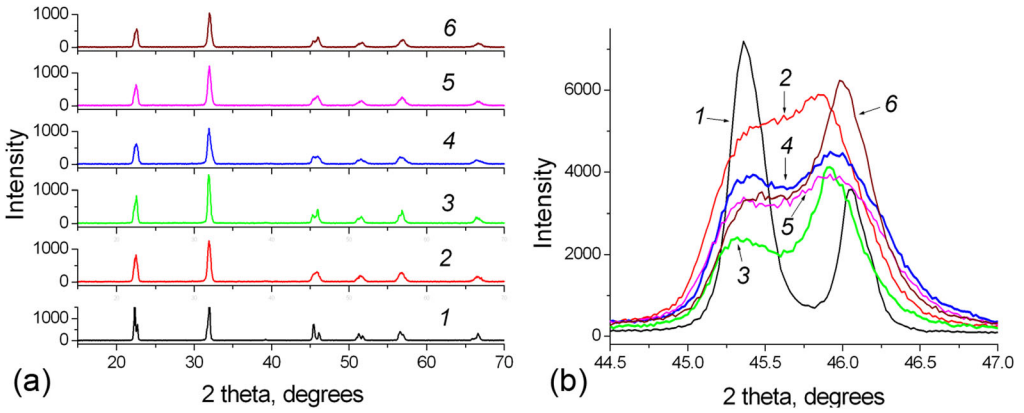

Figure 1. (a) X-ray diffraction patterns of the KNN-NBT samples with $x = 0.0$ (*1*), 0.02 (*2*), 0.04 (*3*), 0.06 (*4*), 0.08 (*5*), and 0.10 (*6*). (b) Parts of the X-ray diffraction patterns of the KNN-NBT samples with *hkl* -200 and 020.

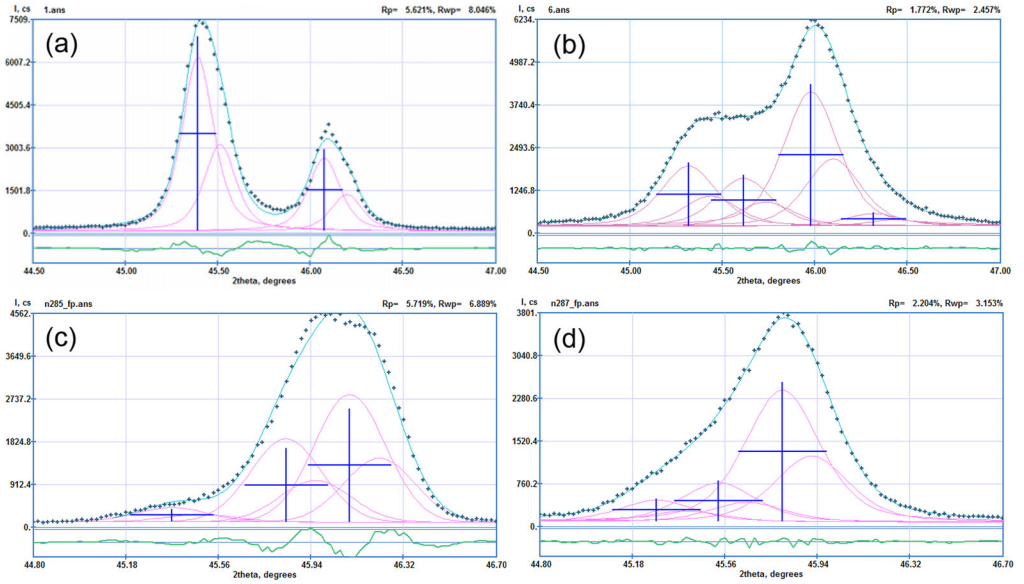

Figure 2. Parts of the X-ray diffraction patterns of the KNN-NBT samples with $x = 0.0$ (a), 0.02 (b), and 0.1 (c); and KNN-BNZ with $x = 0.01$ (d), 0.03 (e), and 0.05 (f) simulated using ProfitVZ program.

In this work, effects of modification of KNN compositions by donor (Bi^{3+}) and acceptor dopants (Ti^{4+} and Zr^{4+}) in the A- and B-sites of perovskite lattice on structure, microstructure, dielectric, ferroelectric, and local piezoelectric properties of ceramic solid solutions $(1\text{-}x)(K_{0.5}Na_{0.5})NbO_3 - x(Bi_{0.5}Na_{0.5})TiO_3$ (KNN-NBT) ($x = 0 \div 0.1$) and $(1\text{-}x)(K_{0.5}Na_{0.5})NbO_3 - x(Bi_{0.5}Na_{0.5})ZrO_3$ (KNN-BNZ) ($x = 0.01 \div 0.05$) have been studied.

2. Experimental

Ceramic samples in the systems $(1\text{-}x)(K_{0.5}Na_{0.5})NbO_3 - x(Bi_{0.5}Na_{0.5})TiO_3$ ($x = 0 \div 0.1$, $\Delta x = 0.01$) and $(1\text{-}x)(K_{0.5}Na_{0.5})NbO_3 - x(Bi_{0.5}Na_{0.5})ZrO_3$ ($x = 0.01$, 0.03, 0.05) were

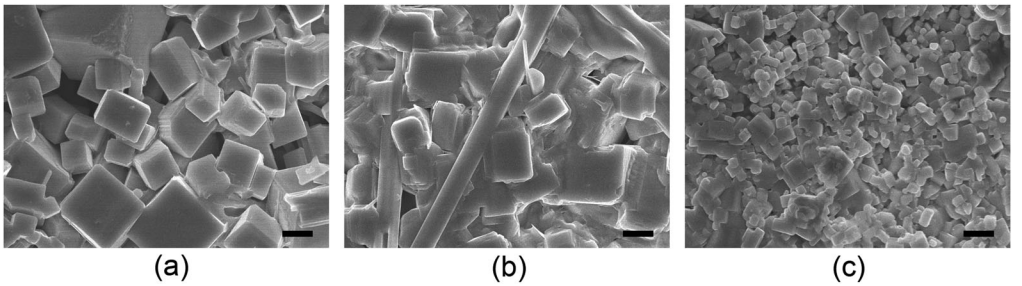

Figure 3. Microstructure of the samples (a) KNN-BNT and (b, c) KNN-BNZ with $x = 0.01$ (a); 0.03 (b), and 0.05 (c). Bars – 2 μm.

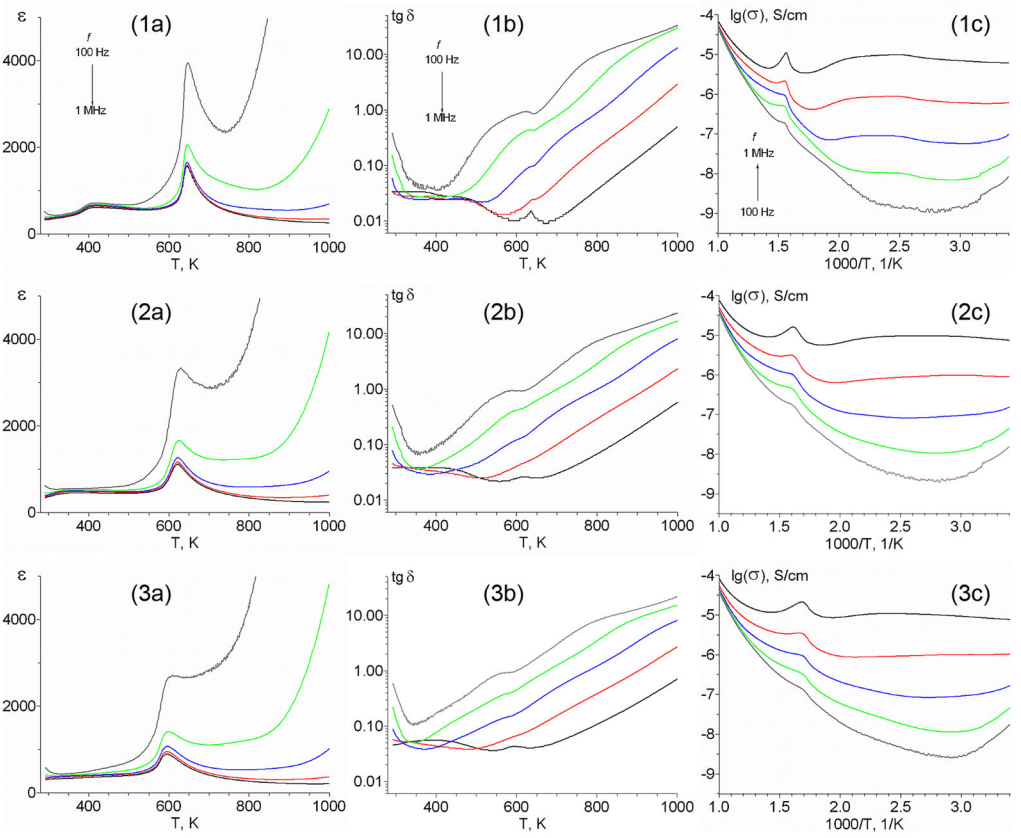

Figure 4. Temperature dependences of (a) dielectric permittivity $\varepsilon(T)$, (b) dielectric loss $\tan\delta(T)$ and (c) electroconductivity of the samples KNN-NBT (*1–3*) with $x = 0.01$ (*1*), 0.03 (*2*), and 0.05 (*3*) measured at frequencies $f = 1$, 10, 100, 300 kHz, and 1 MHz.

prepared by the two-step solid-state reaction method at calcination temperatures of $T_1 = 1070$ K (6 h), and sintering temperatures of $T_2 = 1370 \div 1440$ K (2 h). The samples were additionally modified by small amounts of KCl additives in order to improve sintering of ceramics [22, 25, 26]. Sodium carbonate Na_2CO_3, potassium carbonate K_2CO_3, Nb_2O_5, Bi_2O_3, TiO_2, and ZrO_2 oxides ("pure" grade), and KCl, were used as starting

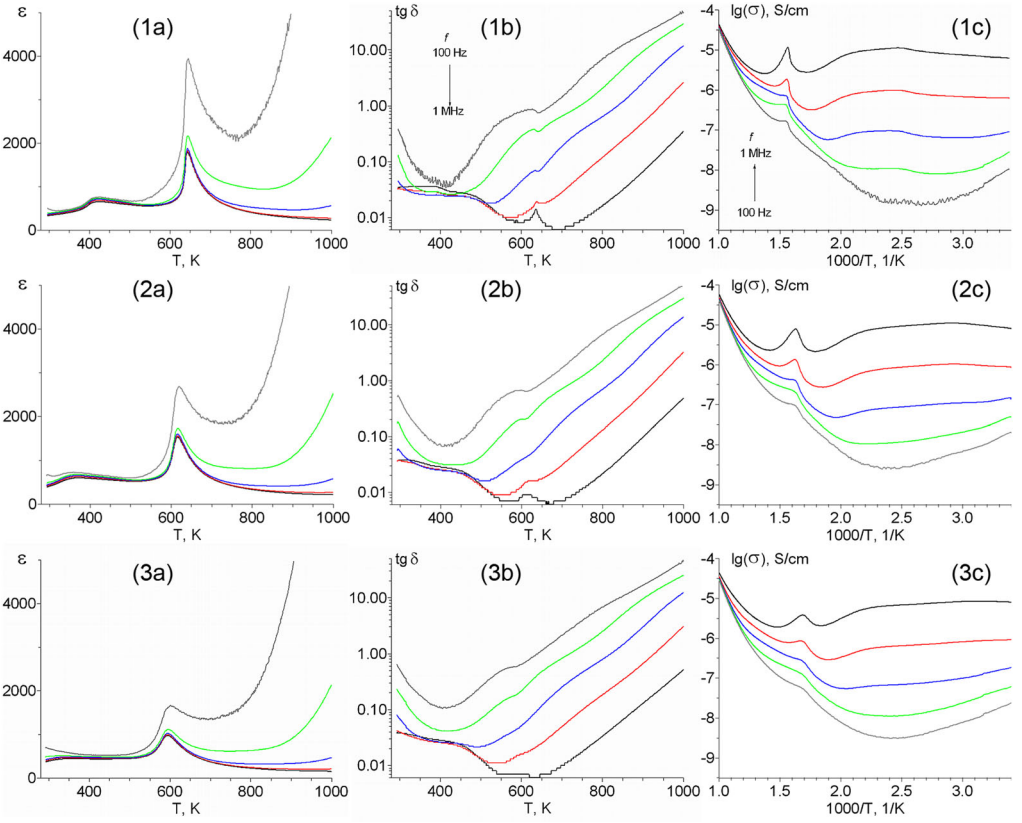

Figure 5. Temperature dependences of (a) dielectric permittivity $\varepsilon(T)$, (b) dielectric loss $\tan\delta(T)$ and (c) electroconductivity of the samples KNN-NBZ (*1-3*) with $x = 0.01$ (*1*), 0.03 (*2*), and 0.05 (*3*) measured at frequencies $f = 1$, 10, 100, 300 kHz, and 1 MHz.

materials. Before synthesis, carbonates were dried at 673 K (2 h) in order to remove absorbed water.

A complex of physicochemical methods was used to characterize phase content and structure parameters, microstructure, ferroelectric, dielectric, and local piezoelectric properties of the samples: the X-ray diffraction (DRON-3M, Cu-K_α radiation with wavelength $\lambda = 1.5405$ A, 2 theta range of $5 \div 70$ degrees), Scanning Electron Microscopy (SEM) (JEOL YSM-7401F with a JEOL JED-2300 energy dispersive X-ray spectrometer system), Differential Scanning Calorimetry (DSC) (SDT Q-600 thermal analyzer with scan rate of 10 K/min), Second Harmonic Generation (SHG) (Nd:YAG laser, $\lambda = 1.064$ μm in the reflection), Dielectric Spectroscopy (DS) (Agilent 4284 A; 1 V) on heating and cooling with 10 K/min. in the temperature interval of $300 \div 1000$ K, and the frequency range of $100\,\text{Hz} \div 1\,\text{MHz}$, and Atomic Force Microscopy (AFM) in Piezoresponse Force Microscopy (PFM) mode (MFP-3D, Asylum Research, USA). Ti/Ir-coated cantilevers (Asyelec-02, Asylum Research, USA) with a radius of curvature ~ 28 nm were used. The PFM out-of-plane images (mixed signal) were scanned in the PFM Dual AC Resonance Tracking (DART) mode at $1 \div 2$ V and a frequency of ~ 980 kHz.

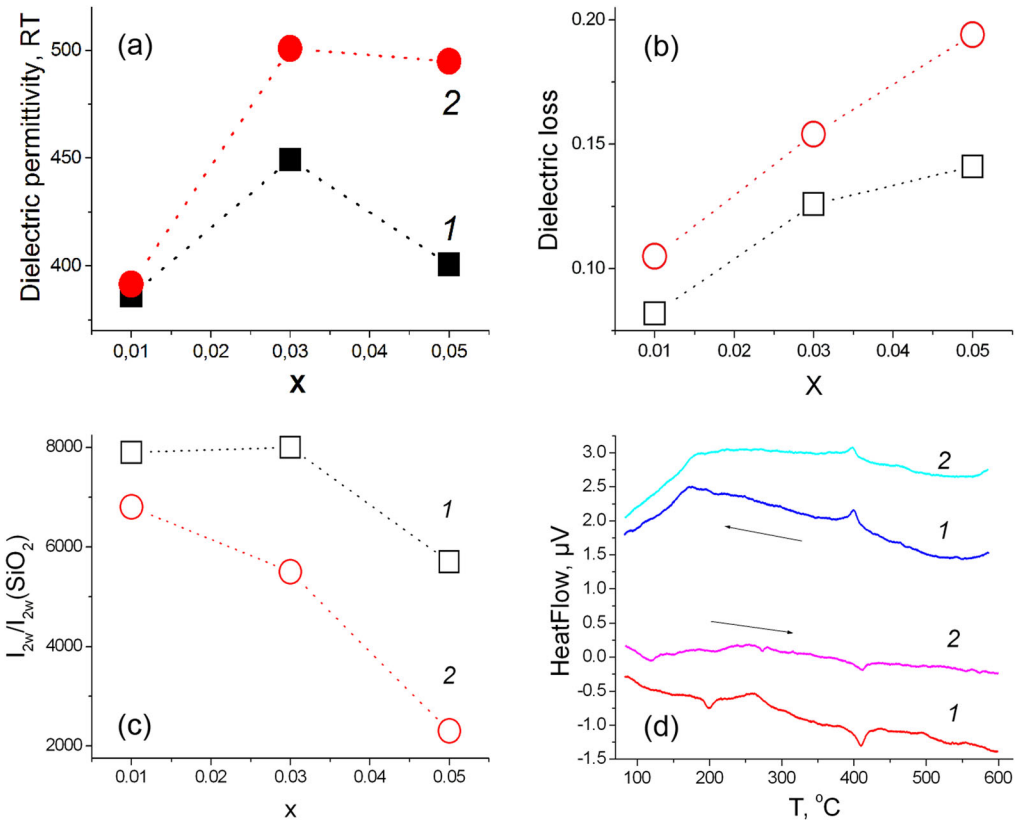

Figure 6. Concentration dependences of (a) dielectric permittivity, (b) dielectric loss, and (c) SHG signal of the samples KNN-NBT (*1*) and KNN-NBZ (*2*) measured at the room temperature at $f = 1$ kHz (a, b). (d) Temperature dependences of the Heat Flow of the samples KNN-NBT with $x = 0.00$ (*1*) and 0.08 (*2*).

3. Results and discussion

Pure ceramic samples with perovskite structure were prepared (Figure 1). Initial KNN samples revealed orthorhombic structure. Introduction of Ti^{4+} cations into B-sites of perovskite lattice led to the formation of MPB, which included phases with different symmetry – O and T (Figure 2a–c). Simulation of separate peaks using ProfitVZ program [27] revealed that BNT additives stimulated transition from O phase to mixture of O and T phases (MPB) and then to T phase (MPB), while in compositions with BNZ additives rhombohedral (R) phase was present (Figure 2d–f). The observed changes in the unit cell volume of the KNN-based ceramics correlated with cation substitutions. Slight decrease in the orthorhombic unit cell parameters was revealed in the samples modified by smaller A-site cations (Bi,Na) and B-site cations (Ti^{4+}). These data confirmed a conclusion on the existence of MPB between O and T ferroelectric phases in the KNN-NBT compositions and between O and R ones in the KNN-BNZ compositions [16, 20].

Microstructure of the samples was sensitive to substitutions and sintering conditions as well (Figure 3). Slight decrease of mean size of grains was observed in KNN-BNZ ceramics with increasing *x*.

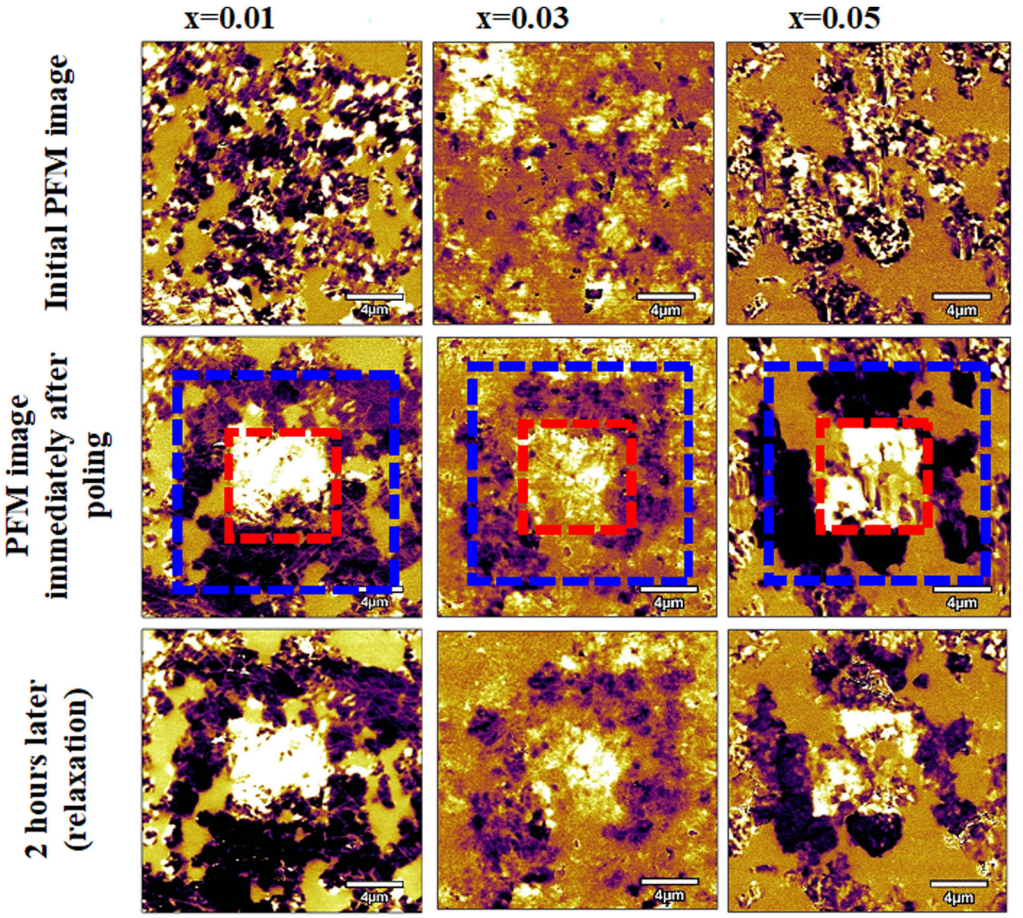

Figure 7. Initial PFM images of KNN-BNT, PFM images immediately after poling, and after 2 hours (relaxation). Blue squares – poling at −30V, red squares – poling at +30V.

Using the dielectric spectroscopy method, steps near $400 \div 300$ K and maxima at $650 \div 600$ K were revealed in the dielectric permittivity versus temperature curves (Figures 4 and 5). Slight decrease in temperatures of both phase transitions was observed in ceramic solid solutions doped by Ti^{4+} or Zr^{4+} cations. Increase in dielectric permittivity at the room temperature was characteristic for the KNN-BNT with $x = 0.03$ and for the KNN-BNZ samples with $x = 0.03 \div 0.05$ (Figure 6a), though dielectric loss increased for all the samples studied (Figure 6b). Using the SHG method, polar nature of the samples indicating their ferroelectric properties was proved, and position of MPB in the KNN-NBT system was confirmed at $x = 0.03$ (Figure 6c). DSC data confirmed slight decrease in T_C value for the KNN-NBT samples (Figure 6d).

PFM method was used to characterize surface morphology, as-grown domain structure, and local piezoelectric hysteresis loops of the samples prepared. Before PFM characterization, the samples were preliminary polished using polycrystalline diamond till the root mean square roughness of the samples reached < 10 nm.

Complex domain structure consisting of multiple domain patterns was found in the investigated ceramics (Figures 7 and 8). In order to study the domain switching

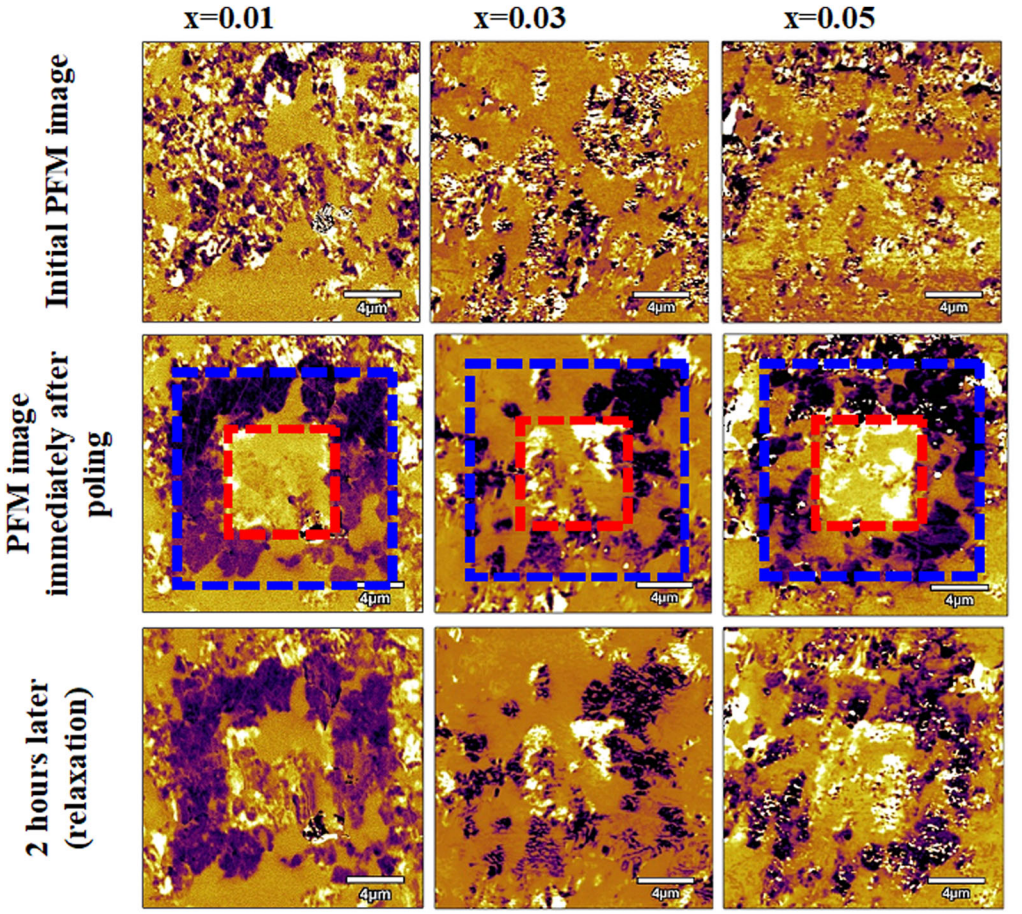

Figure 8. Initial PFM images of KNN-BNZ, PFM images immediately after poling, and after 2 hours (relaxation). Blue squares – poling at -30V, red squares – poling at +30V.

behavior of the KNN ceramics doped with BNT and BNZ additives, we wrote a 7.5×7.5 μm^2 positively polarized domain embedded in a 15×15 μm^2 equivalent negatively polarized domain. Figures 7 and 8 (middle columns) present information of the writing voltage, and the dark and bright areas are obtained by application of –30 V and +30 V DC biases, respectively. Strong PFM contrast suggests complete switching process under poling only for piezoelectric activity grains. Local PFM hysteresis loops observed indicated ferroelectric polarization switching at nanoscale for the samples studied. An AC voltage ($1 \div 2$ V) was superimposed onto a triangular square-stepping wave ($f = 0.5$ Hz, with writing and reading times 25 ms, and bias window up to ± 30 V) during the remnant piezoelectric hysteresis loops measurements. Remnant hysteresis loops were obtained for separate grains (Figure 9). All PFM hysteresis loops are distinctly asymmetric along the axis Y. According to Jesse et al. [28], this offset is mainly attributed to the electrostatic effect. Moreover, the local PFM hysteresis loops account for the polarization switching process in a nanoscale, just below the tip. Therefore, intrinsic polarization in the nanoregion may also contribute to the offset and asymmetry of the local piezoresponse hysteresis loops [29]. Local PFM hysteresis loops revealed

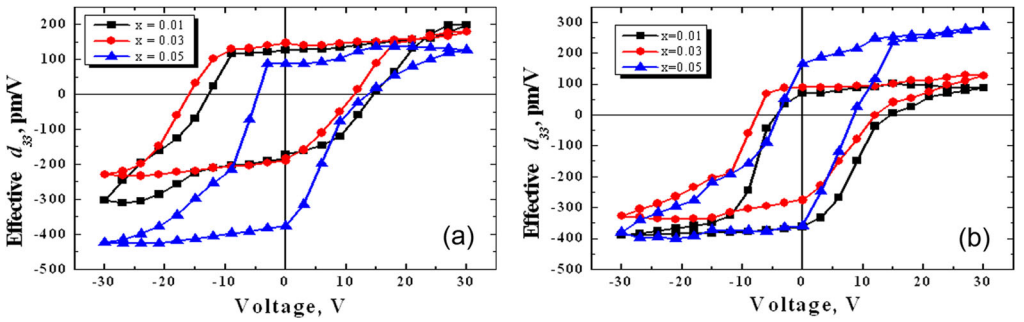

Figure 9. Local PFM hysteresis loops from regions demonstrating larger domain contrast in the VPFM images for the samples (a) KNN-BNT and (b) KNN-BNZ with $x = 0.01$, 0.03, and 0.05.

that d_{33} piezoelectric coefficient reached the highest value of 180 pm/V for the samples KNN-BNT with $x = 0.03$ and 290 pm/V for the samples KNN-BNZ with $x = 0.05$, with the saturation of loops reached at voltage value $\sim$ 30 V. Lower d_{33} value of the samples KNN-BNT may point to influence of acceptor additives hindering the domain walls movement [30, 31].

4. Conclusion

Phase content, structure parameters, microstructure, dielectric, ferroelectric, and local piezoelectric properties of the KNN ceramics doped with BNT and BNZ additives were studied. Slight changes in the unit cell volume, mean size of grains, and temperatures of phase transitions were observed depending on composition. The best saturation loops and high values of effective d_{33} piezoelectric coefficients were observed for the KNN-based ceramics doped by the BNT with $x = 0.03$ and BNZ with $x = 0.05$, thus confirming that these ceramics are promising candidates for lead-free piezoelectric materials development.

Funding

The work was supported by the Russian Foundation for Basic Research (project 18-03-00372). The work was carried out at the expense of a grant allocated by the FITC HP RAS for the implementation of the state task on the topic No. 45.22 (AAAA18-118012390045-2). PFM and SEM studies were performed at the Center for Shared Use "Material Science and Metallurgy" at the National University of Science and Technology "MISiS" and FSRC ≪Crystallography and Photonics≫ RAS and were supported by the Ministry of Higher Education and Science of the Russian Federation within the framework of the State tasks.

References

[1] E. Cross, Lead-free at last, *Nature.* **432**(7013), 24 (2004). DOI: 10.1038/nature03142.
[2] E. Ringaard and T. Wurlitzer, Lead-free piezoceramics based on alkali niobates, *J. Eur. Ceram. Soc.* **25**, 2701 (2005). DOI: 10.1016/j.jeurceramsoc.2005.03.126.
[3] T. Takenaka and H. Nagata, Current status and prospects of lead-free piezoelectric ceramics, *J. Eur. Ceram. Soc.* **25** (12), 2693 (2005). DOI: 10.1016/j.jeurceramsoc.2005.03.125.

[4] T. R. Shrout and S. Zhang, Lead-free piezoelectric ceramics: Alternatives for PZT, *J. Electroceram.* **19** (1), 113 (2007). DOI: 10.1007/s10832-007-9047-0.
[5] H. Du *et al.*, Sintering characteristic, microstructure, and dielectric relaxor behavior of $(K_{0.5}Na_{0.5})NbO_3$-$(Bi_{0.5}Na_{0.5})TiO_3$ lead-free ceramics, *J. Am. Ceram. Soc.* **91** (9), 2903 (2008). DOI: 10.1111/j.1551-2916.2008.02528.x.
[6] T. Takenaka, H. Nagata, and Y. Hiruma, Current developments and prospective of lead-free piezoelectric ceramics, *Jpn. J. Appl. Phys.* **47** (5), 3787 (2008). DOI: 10.1143/JJAP.47.3787.
[7] J. Rodel *et al.*, Perspective on the development of lead-free piezoceramics, *J. Am. Ceram. Soc.* **92**, 1153 (2009). DOI: 10.1111/j.1551-2916.2009.03061.x.
[8] D. Q. Xiao *et al.*, Investigation on the composition design and properties study of perovskite lead free piezoelectric ceramics, *J. Mater. Sci.* **19**, 5408 (2009). DOI: 10.1007/s10853-009-3543-3.
[9] P. K. Panda, Review: environmental friendly lead-free piezoelectric materials, *J. Mater. Sci.* **44** (19), 5049 (2009). DOI: 10.1007/s10853-009-3643-0.
[10] J. Tellier *et al.*, Crystal structure and phase transitions of sodiumpotassium niobate ceramics, *Solid State Sci.* **11** (2), 320 (2009). DOI: 10.1016/j.solidstatesciences.2008.07.011.
[11] Y. Q. Lu and Y. X. Li, A review on lead-free piezoelectric ceramics studied in China, *J. Adv. Dielectr.* **01** (03), 269 (2011). DOI: 10.1142/S2010135X11000409.
[12] J. Fang *et al.*, Narrow sintering temperature window for $(K,Na)NbO_3$-based lead-free piezoceramics caused by compositional segregation, *Phys. Stat. Sol. (A).* **208** (4), 791 (2011). DOI: 10.1002/pssa.201026500.
[13] I. Coondoo, N. Panwar, and A. Kholkin, Lead-free piezoelectrics: Current status and perspective, *J. Adv. Dielectr.* **03** (02), 1330002 (2013). DOI: 10.1142/S2010135X13300028.
[14] J.-F. Li *et al.*, $(K,Na)NbO_3$-based lead-free piezoceramics: fundamental aspects, processing technologies, and remaining challenges, *J. Am. Ceram. Soc.* **96** (12), 3677 (2013). DOI: 10.1111/jace.12715.
[15] Z. Wang *et al.*, New lead-free $(Na_{0.5}K_{0.5})NbO_3$-$X(Bi_{0.5}Na_{0.5})ZrO_3$ ceramics with high piezoelectricity, *J. Am. Ceram. Soc.* **97** (3), 688 (2014). DOI: 10.1111/jace.12836.
[16] J. G. Wu, D. Q. Xiao, and J. G. Zhu, Potassium-sodium niobate lead-free piezoelectric materials: past, present, and future of phase boundaries, *Chem. Rev.* **115** (7), 2559 (2015). DOI: 10.1021/cr5006809.
[17] J. Rodel *et al.*, Transferring lead-free piezoelectric ceramics into application, *J. Eur. Ceram. Soc.* **35**, 1659 (2015). DOI: 10.1016/j.jeurceramsoc.2014.12.013.
[18] B. Malič *et al.*, Sintering of lead-free piezoelelctric sodium-potassium niobate ceramics, *Materials.* **8** (12), 8117 (2015). DOI: 10.3390/ma8125449.
[19] E. D. Politova *et al.*, Influence of NaCl/LiF additives on structure, microstructure and phase transitions of $(K_{0.5}Na_{0.5})NbO_3$ ceramics, *Ferroelectrics.* **489** (1), 147 (2015). DOI: 10.1080/00150193.2015.1070248.
[20] D. Wang *et al.*, Composition and temperature dependence of structure and piezoelectricity in $(1–x)(K_{1-y}Na_y)NbO_3$-$x(Bi_{1/2}Na_{1/2})ZrO_3$ lead-free ceramics, *J. Am. Ceram. Soc.* **100** (2), 627 (2017). DOI: 10.1111/jace.14589.
[21] D. Alikin *et al.*, Ferroelectric domain structure and local piezoelectric properties of lead-free $(Ka_{0.5}Na_{0.5})NbO_3$ and $BiFeO_3$-based piezoelectric ceramics, *Materials.* **10** (1), 47 (2017). DOI: 10.3390/ma10010047.
[22] E. D. Politova *et al.*, Structure and ferroelectric properties of lead-free NBT-KBT-BF ceramics, *Ferroelectrics.* **518** (1), 109 (2017). DOI: 10.1080/00150193.2017.1360614.
[23] J. Rödel and J. Li, Lead-free piezoelectric ceramics: status and perspective, *MRS Bull.* **43** (8), 576 (2018). DOI: 10.1557/mrs.2018.181.
[24] L. Jiang *et al.*, Study of the relationships among the crystal structure, phase transition behavior and macroscopic properties of modified $(K,Na)NbO_3$-based lead-free piezoceramics, *J. Euro. Ceram. Soc.* **38** (5), 2335 (2018). DOI: 10.1016/j.jeurceramsoc.2017.12.062.

[25] E. D. Politova *et al.*, Processing and characterization of lead-free ceramics on the base of sodium–potassium niobate, *J. Adv. Dielectr.* **08** (01), 1850004 (2018). DOI: 10.1142/S2010135X18500042.

[26] E. D. Politova *et al.*, Structure, ferroelectric and piezoelectric properties of KNN-based perovskite ceramics, *Ferroelectrics.* **538** (1), 45 (2019). DOI: 10.1080/00150193.2019.1569984.

[27] V. V. Zhurov and S. A. Ivanov, PROFIT a program for powder diffraction data evaluation for IBM PC with a graphical user interface, *Crystallogr. Rep.* **42**, 239 (1997).

[28] S. Jesse, H. N. Lee, and S. V. Kalinin, Quantitative mapping of switching behavior in piezoresponse force microscopy, *Rev. Sci. Instrum.* **77** (7), 073702 (2006). DOI: 10.1063/1.2214699.

[29] H. Qiao *et al.*, Modulation of electrocaloric effect and nanodomain structure in Mn-doped $Pb(In_{0.5}Nb_{0.5})O_3$-$PbTiO_3$ ceramics, *Ceram. Int.* **44** (16), 20417 (2018). DOI: 10.1016/j.ceramint.2018.08.035.

[30] S. Jesse, A. P. Baddorf, and S. V. Kalinin, Switching spectroscopy piezoresponse force microscopy of ferroelectric materials, *Appl. Phys. Lett.* **88** (6), 062908 (2006). DOI: 10.1063/1.2172216.

[31] H. Trivedi *et al.*, Local manifestations of a static magnetoelectric effect in nanostructured $BaTiO_3$-$BaFe_{12}O_9$ composite multiferroics, *Nanoscale.* **7** (10), 4489 (2015). DOI: 10.1039/C4NR05657D.